Diaminopropionic Acid Reinforced Graphene Sponge and Its Use for Hemostasis

Kecheng Quan,[†,⊥] Guofeng Li,[†,⊥] Lei Tao,[‡] Qian Xie,[§] Qipeng Yuan,[†] and Xing Wang[*,†]

[†]The State Key Laboratory of Chemical Resource Engineering, Beijing University of Chemical Technology, Beijing 100029, P. R. China

[‡]The Key Laboratory of Bioorganic Phosphorus Chemistry & Chemical Biology (Ministry of Education), Department of Chemistry, Tsinghua University, Beijing 100084, P. R. China

[§]Nephrology Department, Peking University Third Hospital, Beijing 100191, P. R. China

ABSTRACT: 2,3-Diaminopropionic acid (DapA), a medicinal amino acid, is used for the first time to prepare a DapA cross-linked graphene sponge (DCGS) for hemostasis treatment. In a comparison with the reported ethanediamine (EDA) cross-linked graphene sponge (CGS), this carboxyl-functionalized DCGS can not only quickly absorb plasma, but also stimulate erythrocytes and platelets to change their normal form and structure at the interface, which largely affects a cell's metabolism and biofunction, thus further promoting blood coagulation. Whole blood clotting and rat-tail amputation tests indicated that on the basis of the additional interfacial stimulation, the hemostatic efficiency of the DCGS has been

significantly improved in comparison with that of the CGS control ($P < 0.05$). In-depth insight revealed that the increased oxidation degree and the negative charge density play the crucial rule in the enhanced hemostatic performance. The chiral effect contributes mainly to the selective adhesion of erythrocytes and platelets rather than practical hemostasis. Nevertheless, this presentation demonstrated that, on the premise of keeping the fast absorbability, this is an effective method to improve the hemostatic efficiency by enhancing the cell/graphene interface interaction.

KEYWORDS: 2,3-diaminopropionic acid, cross-linked graphene sponge, interfacial stimulation, hemostasis, carboxyl-functionalization
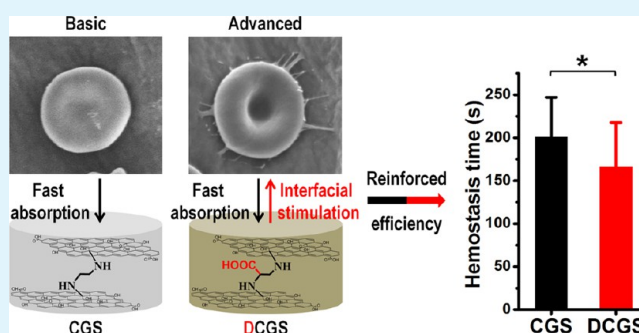
1. INTRODUCTION

Effective hemostatic materials that can rapidly control bleeding are vital to the wound healing or gain time for further rescue, as excessive hemorrhage is the main reason for trauma death both in military and in civilian medicine.[1,2] Some classical hemostatic agents, such as zeolite and mesoporous silica, can quickly absorb the liquid component of blood to promote erythrocytes and platelets to aggregate, resulting in a fast hemostasis.[3−6] On the basis of this hemostatic mechanism, we have also exploited a cross-linked graphene sponge (CGS) with remarkable hemostatic performance recently,[7] which was highlighted due to the trial of graphene-based material in the field of bleeding control. This porous sponge could fast absorb the plasma and thus promote blood clotting on the wound surface. However, it is regrettable that the surface of CGS did not stimulate hemocytes regardless of platelets or erythrocytes. As a result, substantial room for efficiency improvement exists for the performance of bleeding control, which inspired us to further excavate the hemostatic potential of the CGS by reinforcing the cell/graphene interface interaction.

Increasing surface charges is an effective strategy for interfacial stimulation.[8,9] As reported, G. Zbiden et al. demonstrated that negatively charged liposomes could significantly accelerate whole blood clotting time by stimulating

the plasmatic contact activating system.[10] Besides, M. Miyamoto et al. used latex particles to prove that high negative charges could activate platelet stimulant [adenosine diphosphate (ADP)] or coagulation factor (factor III).[11,12] On the basis of the components of the graphene sponge, increasing its carboxyl groups should be a direct and effective method, because those oxygen polar groups can instantly stimulate erythrocytes and platelets when in contact with blood. As reported by Singh et al.,[13−15] atomically thin graphene oxide (GO) rather than reduced graphene oxide (rGO) sheets were highly thrombogenic in mouse and evoked strong aggregatory response in human platelets even on a scale comparable to that elicited by thrombin due to surface charge distribution. In addition, other carboxylated carbon materials (e.g., carbon nanodiamond) were found that they can also activate platelets and induce thromboembolism. Therefore, introduction of sufficient carboxyl groups is a rational strategy to improve the hemostatic efficiency of the typical CGS by reinforcing the cell/graphene interface interaction.
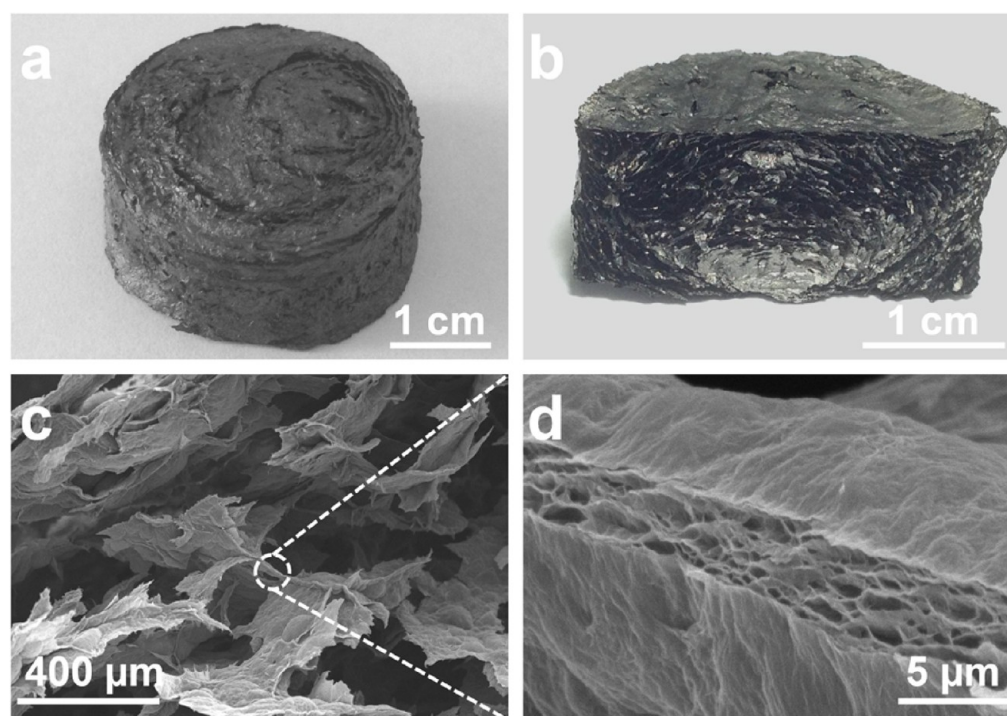
Scheme 1. Schematic Representation of the Preparation Route and the Hemostatic Mechanism[a]
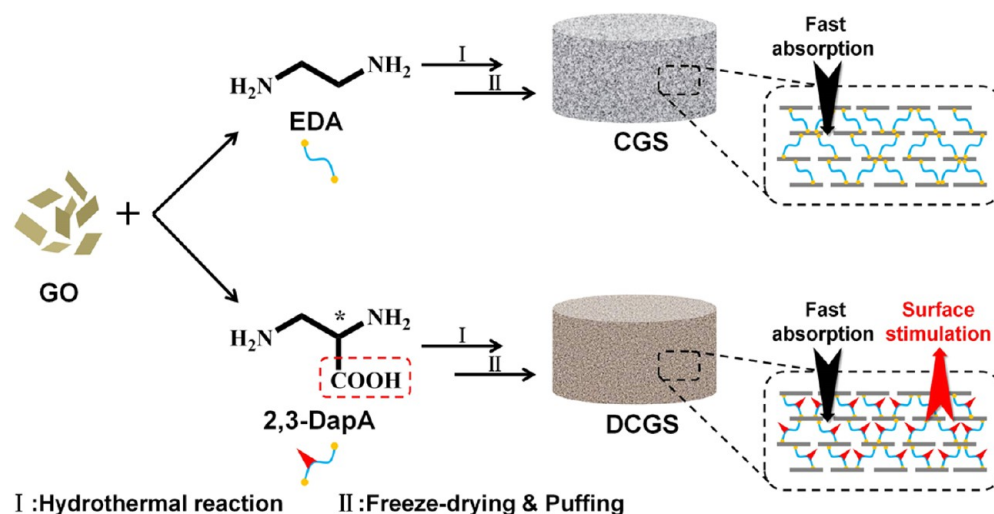
[a]To compare with the CGS, this DCGS is endowed with a new hemostatic mechanism (surface stimulation, marked as red arrow) through the carboxyl-functionalization, owning to the 2,3-DapA linkers.

Figure 1. (a) Photograph of the DCGS (2.6 cm diameter, 1.2 cm thickness). (b) Cross section of the DCGS with a layers stacking structure. (c) SEM image of the interior porous structure of the DCGS. (d) The porous lamellar structure magnified from part c.

2,3-Diaminopropionic acid (2,3-DapA) is a suitable agent. It not only possesses a diamino structure as well as ethanediamine (EDA, the linker in CGS), acting as building block to synthesize the cross-linked construction, but also can increase the oxidation degree and negative charges of the material by its carboxyl group. Furthermore, as the simplest nonproteinogenic α,β-diamino acids, 2,3-DapA has been widely researched for biomedical applications.[16,17] Especially, 2,3-DapA is the synthesis precursor of dencichine (β-N-oxalyl-L-α,β-diaminopropionic acid), which is a famous natural hemostatic agent found in traditional Chinese medicine.[18] Hence, 2,3-DapA should be safe for bleeding control.

Herein, we adopt 2,3-DapA for the first time as the linker to cross-link GO sheets into a new type of black hemostatic sponge (Scheme 1), thus combining two kinds of hemostatic mechanism into one material. To compare with the CGS, this novel 2,3-DapA cross-linked graphene sponge (DCGS) inherits the porous structure that could quickly absorb liquid as well; more importantly, the introduction of 2,3-DapA yields the interfacial stimuli between the DCGS and erythrocytes and platelets, thus reinforcing the hemostatic efficiency of this new DCGS. Moreover, as a chiral amino acid,[19−22] the chiral effect of 2,3-DapA within the DCGS is also investigated.

2. EXPERIMENTAL SECTION

2.1. Materials. Graphite powder (80 mesh) was purchased from Qingdao Jinrilai Co., Ltd., Shandong, China. Sulfuric acid (H_2SO_4, 98%), potassium permanganate ($KMnO_4$, 99.9%), sodium nitrate ($NaNO_3$, AR), hydrochloric acid (HCl, 37%), and hydrogen peroxide (H_2O_2, 30%) were purchased from Sigma-Aldrich Company. 2,3-Diaminopropionic acid (DL-, L-, D-, 95%) was purchased from Tokyo Chemical Industry (TCI). 3-(4,5-Dimethyldiazol-2-yl)-2,5-diphenyl tetrazolium bromide (MTT) was purchased from Simcere, Jiangsu, China. L-929 mouse fibroblast cells were supported by the Key Laboratory of Bioorganic Phosphorus Chemistry & Chemical Biology, Tsinghua University. Other reagents were purchased from Sinopharm Chemical Reagent Co., Ltd.

2.2. Preparation and Characterization. A 308 mg portion of 2,3-DapA (raceme or enantiomers), which is equal to the molar weight of EDA used in the CGS synthesis,[7] was diluted into 2 mL ammonium hydroxide. Then the mixture was added into 20 mL of GO solution (3 mg mL^{-1}, prepared via a modified Hummers' method[23]). After a hydrothermal reaction (96 °C, 6 h), the hydrogel was freeze-dried for 48 h and followed by an alcohol washing for another 48 h to remove the unreacted 2,3-DapA. Finally, the DCGS (2.6 cm diameter, 1.2 cm thickness, Figure 1a) was obtained under 800 W microwave puffing for 5 s.[24]

The liquid absorbability of the DCGS was evaluated by measuring the absorption ability and the absorption rate. The absorption ability was measured by the following equation: value = $(m_2 - m_1)/m_1$, where m_1 means the initial weight of the DCGS and m_2 means the weight after adequately absorbing water. The absorption rate was characterized by a high speed camera to observe the whole process showing that a droplet of liquid was absorbed by the DCGS.[7] All of the materials used here are integrated DCGS as shown in Figure 1a, and the initial weight of DCGS is 54.5 ± 5.5 mg.

Scanning electron microscopy (SEM, S-4700 Hitachi) was used to observe the interior structure of the DCGS. Dye adsorption test was completed to measure the specific surface area of the DCGS by the Shi group's methylene blue method,[25] which is modified from a standard method for graphitic materials.[26] Energy-dispersive spectroscopy (EDS, S-4700 Hitachi) was used to observe the surface element content between the DCGS and the CGS. Elemental analysis (EA, Vario ELcube) was used to analyze the elementary composition difference between the DCGS and the CGS. ζ-Potential (Malvern NanoSizer ZS2000) was used to detect the negative potential of the DCGS and the CGS; each sample was repeated 6 times to take the average value.

2.3. Interfacial Interaction between Blood Cells and Material. For a cell morphology test, a drop of anticoagulant citrate dextrose (ACD) whole blood was added onto the DCGS (3 cm diameter, 1.2 cm thickness). The material was incubated for 3 min at 37 °C. Then, the sample was rinsed with phosphate buffer solution (PBS; pH 7.4) 3 times to remove the physically adhered cells and immobilized with 2.5% glutaraldehyde for 2 h. Then, blood cells were dehydrated with 50%, 60%, 70%, 80%, 90%, and 100% ethanol, each for 10 min. Before SEM observation, freeze-drying and metal-spraying processes were finished.

For cell selective adhesion test, a single layer of material (1 × 1 cm^2, 0.25 cm thickness) was immersed in PBS to equilibrate for 2 h at 37 °C. Then, erythrocyte suspensions or platelet rich plasma (PRP) was added into PBS by the volume ratio of 1:20. Then, the blended system was in full contact with the DCGS for another hour at 37 °C. The sample was then treated with the above-mentioned method before SEM observation.[27,28]

2.4. Whole Blood Clotting Evaluation. The whole blood clotting test was completed on the basis of the reported literature.[29−31] A 50 μL portion of recalcified whole blood solution (per 100 μL blood with 8 μL $CaCl_2$, 0.2 M) was added into the isometric DCGS and CGS (1 × 1 × 1 cm^3), respectively, in a glass dish. As a negative control, 50 μL of recalcified whole blood in a glass dish without material was served. Each sample reacted with blood for 60, 90, 120, and 150 s. Then 10 mL of distilled water was added to stop the reaction and to dissolve the hemoglobin in free erythrocytes. The content of hemoglobin in solution was measured by an ultraviolet spectrophotometer (MAPADA UV-1100 spectrophotometer) at 542 nm by the following equation: hemoglobin absorbance = I_s/I_r × 100%, where I_s represented the absorbance of sample and I_r represented the absorbance of the reference value. As a reference value, 50 μL of unreacted recalcified blood was dropped directly in 10 mL of distilled water to measure its ultraviolet absorption value. This experiment was repeated 6 times under the same condition.

2.5. Rat-Tail Amputation. Surgery was completed on 7-week-old Sprague−Dawley (SD) rats (weight of 200−250 g, Vital (Charles) River Laboratory, Beijing, China). Animals were treated and cared for in accordance with the National Research Council's Guide for the care and use of laboratory animals. Anesthesia was induced with 10% chloral hydrate (0.5 mL per 100 g weight of animal). 50% length of the tail was cut by surgical scissors. After cutting, the tail of the rat was placed in air for 15 s to ensure normal blood loss. Then the wound was covered with the DCGS (2.6 cm diameter, 1.2 cm thickness) under slight pressure. The data of bleeding time and blood loss was recorded during the hemostatic process. Six parallel groups were tested here to take an average value, and the gauze sponge was used here as a negative control.

2.6. Cytotoxicity Evaluation. This experiment was carried here by a leaching pattern. First, the RPMI-1640 medium was added into materials (CGS, DCGS, L-DCGS, and D-DCGS), respectively, at the ratio of 10 mg mL^{-1} for full contact. After 24 h, the obtained impregnating solution was used as complete medium (CM) being mixed with 10% (v/v) fetal bovine serum (FBS) and 1% (v/v) antibiotics (100 units mL^{-1} penicillin and 100 units mL^{-1} streptomycin), which served as test group, while the CM with unreacted RPMI-1640 medium served as control group. Then, L929 mouse fibroblast cells (purchased from Cell Resource Center, IBMS, CAMS/PUMC, Beijing, China) in a logarithmic growth phase were incubated in CM at 37 °C in a humidified air condition of 5% (v/v) CO_2. After another 24 h, the cells were cultured in 5 mg/mL 3-(4,5-dimethylthiazol-2-yl)-2,5-diphenyltetrazolium bromide (MTT) solutions for another 4 h at 37 °C. Then the absorbance of formazan dissolved in DMSO was measured at 570 nm with an ultraviolet spectrophotometer (MAPADA UV-1100 spectrophotometer).[15,32,33] The relative growth rate (RGR) of cells cultured in each group was measured to calculate the cell viability via the following formula: RGR (%) = $Abs_{490\ test}/Abs_{490\ control}$ × 100%. Finally, the toxicity grade of each material was assessed.

3. RESULTS AND DISCUSSION

3.1. Material Characterization. Figure 1a shows the typical DCGS hemostatic sponge, which was prepared with our previous reported method.[7] Though the carboxyl-containing linkers (DapA) were adopted, this graphene sponge perfectly inherited the architectural features of the CGS such as the hierarchical porous structure and high specific surface area (Figure 1b). In particular, Figure 1c exhibits the SEM image of the porous cavity interior structure in the DCGS. An unordered sheet distribution can be found clearly. Due to the puffing process, the stacked GO layers were further separated from each other, thus significantly increasing the specific surface area of the graphene sponge (Figure 1d). According to the methylene blue (MB) method,[25,26] the specific surface area of the DCGS (899.6 ± 60.7 m^2 g^{-1}) was found to be similar to that of the CGS (854.9 ± 30.3 m^2 g^{-1}). No significant difference was observed. The DapA linkers did not change the above-mentioned physical characteristics of the black graphene sponge.

However, obvious changes have taken place in the chemical component of the DCGS due to the presence of the DapA linkers. To compare with the CGS, EDS characterizations (Figure 2a,b) showed a distinct difference for the element
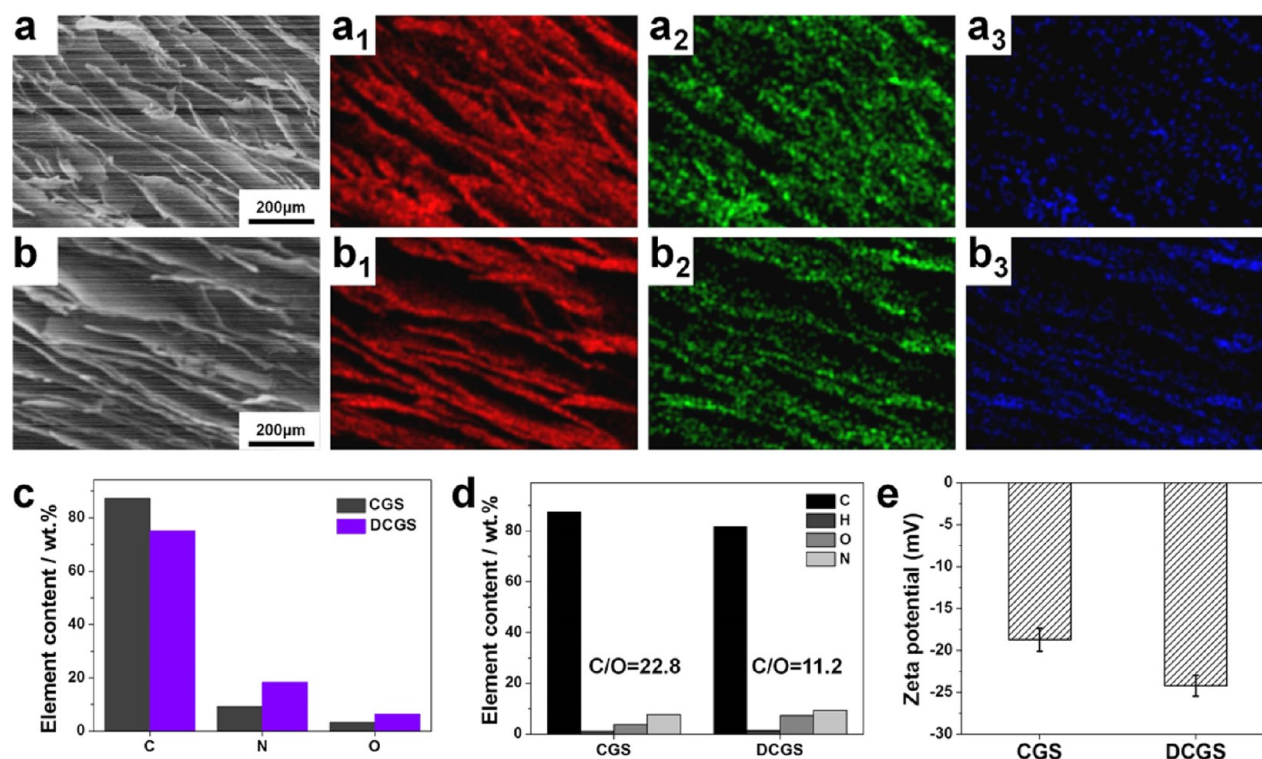
Figure 2. (a) Cross-section SEM image of the CGS and the corresponding EDS mapping of C (a$_1$), N (a$_2$), and O (a$_3$) elements. (b) Cross-section SEM image of the DCGS and the EDS mapping of C (b$_1$), N (b$_2$), and O (b$_3$) elements. (c) The surface element content between the CGS and the DCGS measured from parts a and b. (d) Elemental analysis of the whole CGS and DCGS. (e) ζ-Potential of the CGS and the DCGS in PBS solution ($n = 6$, data values corresponded to mean $\pm$ SD).

content of the DCGS on the cross-sections. Apparently in an equal area, the distribution of C element in the DCGS is less than that in the CGS, while the distributions of N and O elements are observably increased (Figure 2a$_1$−a$_3$,b$_1$−b$_3$), indicating that DapA is uniformly distributed throughout the DCGS. Figure 2c shows the corresponding data analysis. Moreover, the element content of the whole sponge was checked by EA analysis. As shown in Figure 2d, the content of C element is decreased from CGS 87.4% to DCGS 81.8%, while the O element is increased from CGS 3.8% to DCGS 7.3%. This change agrees with the EDS result. Remarkably, the C/O mass ratio presents a decline from CGS 22.8 to DCGS 11.2, indicating the number of oxygenic groups in the DCGS is far more than that in the CGS. As a result, the surface charge density (Figure 2e) demonstrates an expected growth of electric negative potential from −18.7 ± 1.4 to −24.2 ± 1.3 mV. We deduced that these property changes would accelerate blood coagulation, since negative charges are beneficial to activating the clotting factors in the platelet[11−13] and the hydrophilic carboxyl groups are apt to bring damage to the platelet.[9,10,14]

3.2. Material Properties. The liquid absorbability of the DCGS is a key point for the hemostatic application. On the basis of the reported method,[7] the DCGS could absorb more than 10^2 order times the weight of liquid (115.1 ± 17.9 times of water and 114.9 ± 21.2 times of blood), which is close to that of the CGS (112.0 ± 14.1 times that of water and 147.0 ± 17.5 times that of blood). Similarly, the liquid absorption rate of the DCGS was tested to be no less than that of the CGS, where a droplet of blood or water could also be absorbed within 40 ms,[7] indicating the excellent liquid absorbability of the DCGS.[34,35]

The new emerging impact factor for hemostasis within the DCGS is the carboxyl-functionalization. The increase in negative charges has a prominent action for blood clotting.[10−12]

Thus, tests in vitro were first carried out to explore the interfacial effect for erythrocytes and platelets.[27,28] A drop of ACD−whole blood was added into the PBS solution, in which a piece of the DCGS was immersed. This experimental schematic is presented in Figure 3a for a clear understanding. Different from the CGS,[7] the DCGS can obviously impact erythrocytes and platelets to change their physiological states. As shown in Figure 3b, some erythrocytes stretch out pseudopodia on the DCGD surface, though a large amount of erythrocytes disperse on the surface, and most of them keep morphology integrated. In an enlarged SEM image (Figure 3b′), we can see that those pseudopodia are physiologically bonded with the DCGS, and there are no redundant cells stacking with the activated cell. This indicates that the cell is stimulated by the interface of the DCGS rather than aggregation. Furthermore, platelet attachment was tested under the same condition. As shown in Figure 3c,c′, platelets adhered on the surface of the DCGS sprawled with pseudopodia stretching, activated by the interfacial stimulation as well.

In addition, a small quantity of ACD−whole blood (far less than the absorbability of the DCGS) was dropped onto the DCGS to complete the morphology test, as schematically shown in Figure 3d. The plasma was quickly absorbed by the DCGS, leaving a layer of blood cells gathered on the surface. SEM image (Figure 3e) showed that those gathered blood cells altered morphology and clotted locally, forming a thick layer of blood scab (thickness approximately 10 μm, Figure 3e′). This result demonstrated the significant phenomenon that the fast
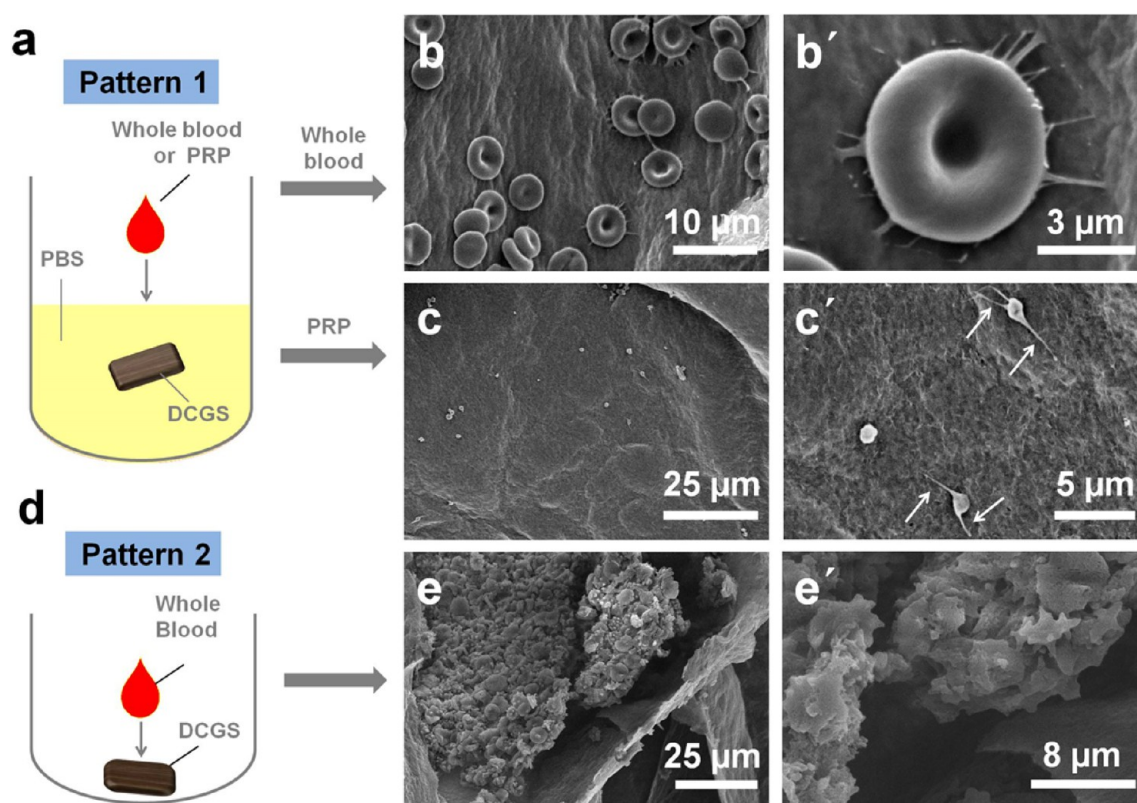
Figure 3. SEM images of interfacial interaction between blood cells and the DCGS. (a and d) Schematic illustration of two kinds of evaluation model. For pattern 1, a droplet of whole blood or PRP was added into PBS solutions; thus, erythrocytes or platelets could selectively adhere on the surface of the DCGS. For pattern 2, a droplet of whole blood was directly dropped onto the DCGS; thus, hemocytes were forced to adhere to it. (b and c) Erythrocyte and platelet selective adhesion experiments completed by pattern 1. (e) Images of cell morphology test completed by pattern 2. (b′, c′, and e′) Magnified image for local observation.

absorbability of the DCGS can promote cruor to achieve rapid hemostatic effect. As is known, activated platelets can release ADP and thromboxane A2, which accelerate recruitment of new platelets to aggregate to accelerate coagulation cascade.[28,36]

All these above-mentioned phenomena illustrated that the porous structure of the DCGS assured the absorbability to fast absorb plasma to promote blood clotting, while the carboxyl-functionalization reinforced the interfacial stimulation to erythrocytes and platelets. Actually, the reinforced stimulation was expected to further accelerate blood coagulation in the process of bleeding control.

3.3. Chiral Effect. 2,3-DapA is a chiral molecule. The chiral effect of biomaterials can impact the adhesion behavior of cells and the protein adsorption on the surface.[19−22] Therefore, L-DapA and D-DapA were used as the linkers to fabricate the chiral graphene sponges, L-DCGS and D-DCGS, respectively. These different chiral materials may perform disparate impact.

We used the L-DCGS and the D-DCGS to repeat the tests performed in section 3.2, observing the difference in cell adhesion. In the cell morphology test (shown in Figure 3d), we have not observed the significant difference between the L-DCGS (Figure 4a) and the D-DCGS (Figure 4b), because blood cells were forced to stay on the material surfaces under this evaluation method. While in the cell selective adhesion test (shown in Figure 3a), it can be noticed that the blood cells exhibit very distinct behaviors on the different enantiomer-formed surfaces (Figure 4c/d and e/f). On the basis of the statistical analysis (t-test), the quantity of adhered cells on the

D-DCGS is approximately 3 times that of the L-DCGS (Figure 4g), and the number of platelets adhered on the D-DCGS is approximately 2 times that of the L-DCGS (Figure 4h). These results illustrate that the cell adhesion behavior is highly influenced by chiral interfaces during a solution environment. Both erythrocytes and platelets are easier to adhere and grow on the D-DCGS compared with the L-DCGS. This difference may affect the hemostatic efficiency of the sponges to a certain extent.

3.4. Hemostatic Performance. As a preliminary performance evaluation, recalcification test[29−31] was evaluated here to compare the coagulation efficiency between the DCGS and the CGS. The recalcification time of the DCGS was found to be approximately 90 s, nearly 30 s shorter than that of the CGS (t-test, $p < 0.05$, $n = 6$), indicating the preponderance of the DCGS in blood coagulation, where the natural recalcification time was approximately 150 s in the control experiment.

Moreover, the rat-tail amputation model was employed as an in vivo evaluation. Figure 5a shows that the mean hemostasis time of the DCGS is 166.0 ± 51.8 s, a 35.0 s reduction compared to that of the CGS (201.0 ± 46.0 s), and the mean blood loss (Figure 5b) of the DCGS exhibits a related decrease to compare with the CGS. These results agree with the above recalcification test.

Furthermore, the chiral effect was investigated by using the L-DCGS and the D-DCGS, demonstrating whether the cell adhesion difference on the above chiral interfaces would influence the hemostatic efficiency. To our regret, no difference was observed for the hemostatic efficiency between the L-
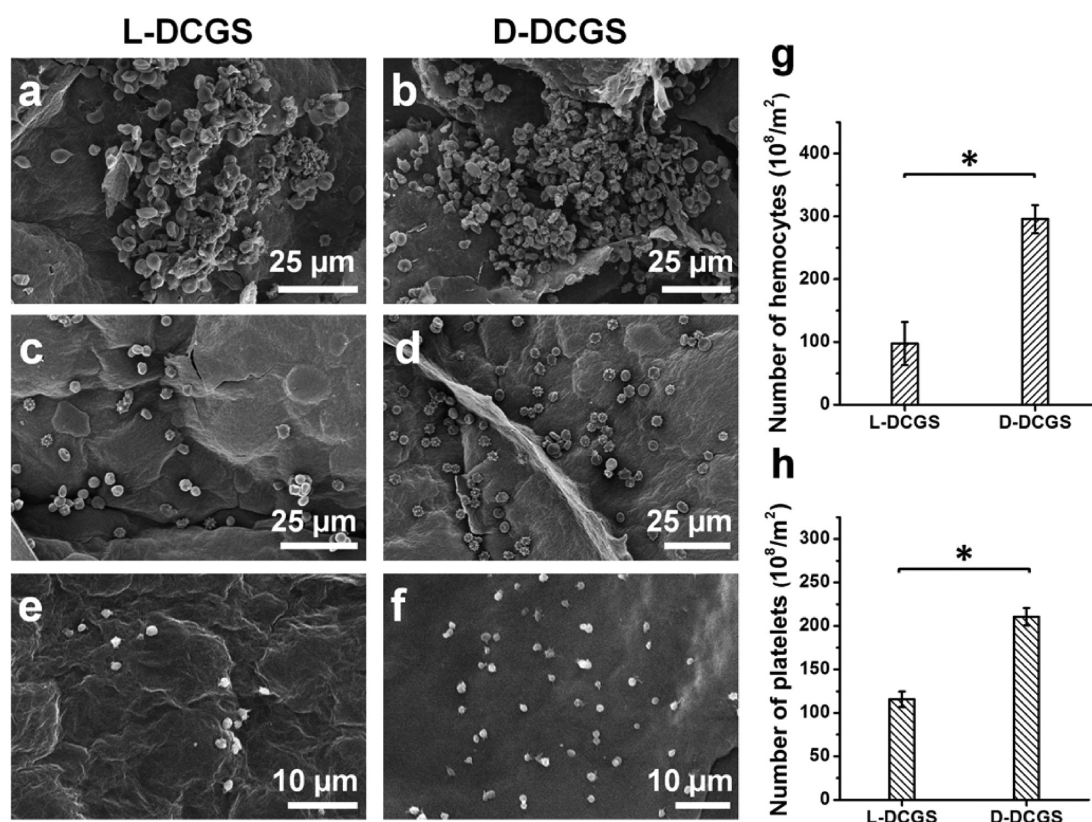
Figure 4. (a and b) Images of cell morphology test between the L- and the D-DCGS. (c and d) Hemocyte selective adhesion test. (e and f) Platelet selective adhesion test. (g) Adhesion number of hemocytes between parts c and d. (h) Adhesion number of platelets between parts e and f. Data values corresponded to mean ± SD ($n = 6$). * represents significant difference between the enantiomers ($P < 0.05$).
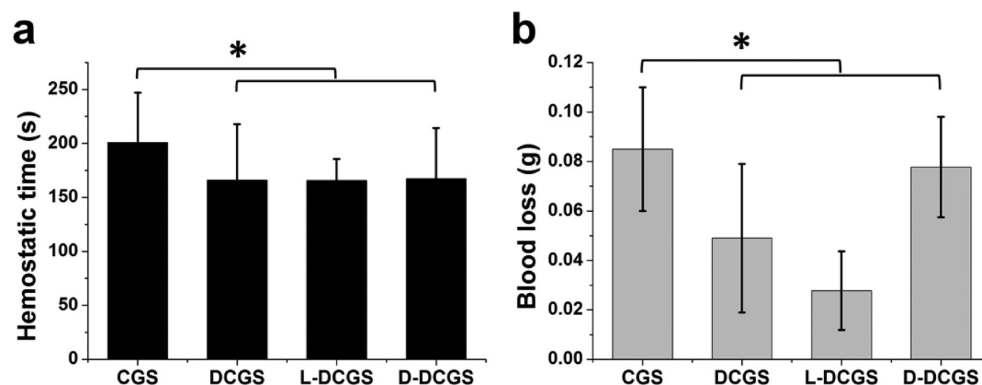
Figure 5. Data from the rat-tail amputation model among the CGS, DCGS, L-DCGS, and D-DCGS. (a) Hemostasis time. (b) Blood loss. Data values corresponded to mean ± SD, $n = 6$. * means $p < 0.05$ and represents a significant difference compared with the CGS.

DCGS (165 ± 20 s, $n = 6$) and the D-DCGS (167 ± 52 s, $n = 6$), which was proximate to the racemate DCGS (Figure 5a). The erythrocytes and platelets adhesion difference on two chiral interfaces (Figure 4) was not reflected in these experimental data. It seems to be a discrepancy here. However, different from the selective adhesion in the solution environment, by the fast absorption in real hemostasis, all of the blood cells were forced to aggregate on the material surface. Thus, the selectivity for the chiral interface disappeared as shown in Figure 4a,b. In other words, a chiral effect could not affect the hemostatic efficiency. A fast absorption mechanism played a key role during the hemostatic process, where the interfacial stimulation mainly depended on the carboxyl-functionalization rather than on the molecular conformation. Although the

hemostatic times of the L-DCGS and the D-DCGS are similar, the blood losses are different (Figure 5b). The weight of blood loss in the L-DCGS is less than that in the D-DCGS and the DCGS. These phenomena may be caused by the adhesion difference of blood cells in chiral interfaces. As blood cells tend to adhere on the D-DCGS, once blood has coagulated, the scab between the wound and the material is inclined to adhere on the material (the D-DCGS). On the contrary, the scab is inclined to adhere on the wound when using the L-DCGS, which is in accordance with the chiral effect discussed in section 3.3.

All of the above-mentioned experiments proved that the interfacial stimulation of the DCGS could further enhance the hemostatic efficiency. On one hand, during the actual

hemostasis process, the hydrophilic carboxyl groups on the DCGS surface could continuously stimulate erythrocytes and platelets that have been separated with the plasma based on the adsorption-concentration process. On the other hand, the surface negative charges of the DCGS could also be active clotting factors in a platelet thus promoting the coagulation cascade.[10−12] Although a 35 s shortage of bleeding time is not able to bring a qualitative leap for the hemostatic properties, the proposed double mechanism (fast absorption and interfacial stimulation) hemostasis within the DCGS is a brand-new concept for a graphene-based sponge.

3.5. Cytotoxicity Evaluation. An MTT assay[32,33] was used to evaluate the cell cytotoxicity of the DCGSs. As shown in Figure 6, the relative growth rates of the DCGS, the L-DCGS,
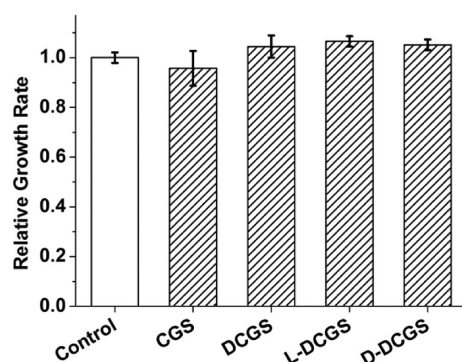
Figure 6. Results of the MTT assay among CGS, DCGS, L-DCGS, and D-DCGS. Data values corresponded to mean ± SD ($n = 6$, $P < 0.05$).

and the D-DCGS are 104.5 ± 4.5%, 106.5 ± 2.1%, and 105.1 ± 2.1%, respectively. The difference is observed to compare with the CGS (95.7 ± 7.0%).[7] As extensively reported,[37,38] when the materials are very biocompatible, it is a normal state that the relative growth rate is higher than 100% because the cells multiply at a rapid rate in the leach liquor. The MTT assay results indicated that all of the DCGSs are noncytotoxic to cells and can be a potential trauma hemostatic.

4. CONCLUSION

In summary, we used DapA as a linker to fabricate a new graphene-based hemostatic sponge (DCGS). To compare with the reported CGS, the carboxyl-functionalized DCGS not only inherits the remarkable liquid absorbability from the CGS, but also enhances the interfacial stimulating ability to blood cells. SEM images for checking the interaction between materials and blood cells have confirmed that the DCGS could stimulate erythrocytes and platelets to alter their morphology due to the increased negative surface charge. As a result, the hemostatic efficiency of the DCGS is 35 s shorter than that of the CGS. In addition, as DapA is a chiral molecule, the chiral effect was demonstrated on blood cell adhesion rather than hemostatic performance. Those results indicated that although the erythrocytes and platelets preferred to adhere on the D-type interface (the D-DCGS), the hemostatic efficiency of two enantiomers (the D-DCGS and the L-DCGS) was not affected by the chiral signals, as fast absorption is the predominant mechanism in this system. On the basis of the above contributions, we believe that this work not only provides a new direction for the development of graphene-based hemostatic materials by using a double (or multi) mechanism

for hemostasis, but also presents a new understanding of chiral materials for use in the field of bleeding control.

■ AUTHOR INFORMATION

Corresponding Author
*E-mail: wangxing@mail.buct.edu.cn.
Author Contributions
[⊥]K.Q. and G.L. contributed equally to this work.
Notes
The authors declare no competing financial interest.

■ REFERENCES

(1) Alam, H. B.; Koustova, E.; Rhee, P. Combat Casualty Care Research: From Bench to the Battlefield. *World J. Surg.* **2005**, *29*, S7−S11.
(2) Alam, H. B.; Burris, D.; DaCorta, J. A. Hemorrhage Control in the Battlefield: Role of New Hemostatic Agents. *Mil. Med.* **2005**, *170*, 63−69.
(3) Ahuja, N.; Ostomel, T. A.; Stucky, G. D.; Conran, R.; Chen, Z.; Al-Mubarak, G. A.; Velmahos, G.; deMoya, M.; Alam, H. B. Testing of Modified Zeolite Hemostatic Dressings in a Large Animal Model of Lethal Groin Injury. *J. Trauma* **2006**, *61*, 1312−1320.
(4) Kozen, B. G.; Kircher, S. J.; Henao, J.; Godinez, F. S.; Johnson, A. S. An Alternative Hemostatic Dressing: Comparison of CELOX, HemCon, and QuikClot. *Acad. Emerg. Med.* **2008**, *15*, 74−81.
(5) Dai, C.; Yuan, Y.; Liu, C.; Wei, J.; Hong, H.; Li, X.; Pan, X. Degradable, Antibacterial Silver Exchanged Mesoporous Silica Spheres for Hemorrhage Control. *Biomaterials* **2009**, *30*, 5364−5375.
(6) Dai, C.; Liu, C.; Wei, J.; Hong, H.; Zhao, Q. Molecular Imprinted Macroporous Chitosan Coated Mesoporous Silica Xerogels for Hemorrhage Control. *Biomaterials* **2010**, *31*, 7620−7630.
(7) Quan, K.; Li, G.; Luan, D.; Yuan, Q.; Tao, L.; Wang, X. Black Hemostatic Sponge Based on Facile Prepared Cross-linked Graphene. *Colloids Surf., B* **2015**, *132*, 27−33.
(8) Ostomel, T. A.; Shi, Q.; Stoimenov, P. K.; Stucky, G. D. Metal Oxide Surface Charge Mediated Hemostasis. *Langmuir* **2007**, *23*, 11233−11238.
(9) Dobrovolskaia, M. A.; Patri, A. K.; Simak, J.; Hall, J. B.; Semberova, J.; De Paoli Lacerda, S. H.; McNeil, S. E. Nanoparticle Size and Surface Charge Determine Effects of PAMAM Dendrimers on Human Platelets in vitro. *Mol. Pharmaceutics* **2012**, *9*, 382−393.
(10) Zbinden, G.; Wunderli-Allenspach, H.; Grimm, L. Assessment of Thrombogenic Potential of Liposomes. *Toxicology* **1989**, *54*, 273−280.
(11) Miyamoto, M.; Sasakawa, S.; Ozawa, T.; Kawaguchi, H.; Ohtsuka, Y. Platelet Aggregation Induced by Latex Particles: I. Effects of Size, Surface Potential and Hydrophobicity of Particles. *Biomaterials* **1989**, *10*, 251−257.
(12) Miyamoto, M.; Sasakawa, S.; Ozawa, T.; Kawaguchi, H.; Ohtsuka, Y. Mechanisms of Blood Coagulation Induced by Latex Particles and the Roles of Blood Cells. *Biomaterials* **1990**, *11*, 385−388.
(13) Singh, S. K.; Singh, M. K.; Nayak, M. K.; Kumari, S.; Shrivastava, S.; Gracio, J. A.; Dash, D. Thrombus Inducing Property of Atomically Thin Graphene Oxide Sheets. *ACS Nano* **2011**, *5*, 4987−4996.
(14) Kumari, S.; Singh, M. K.; Singh, S. K.; Gracio, J.; Dash, D. Nanodiamonds activate blood platelets and induce thromboembolism. *Nanomedicine* **2014**, *9*, 427−440.

(15) Singh, S. K.; Singh, M. K.; Kulkarni, P. P.; Sonkar, V. K.; Gracio, J.; Dash, D. Amine−Modified Graphene: Thrombo−Protective Safer Alternative to Graphene Oxide for Biomedical Applications. *ACS Nano* **2012**, *6*, 2731−2740.

(16) Yegani, R.; Hirozawa, H.; Teramoto, M.; Himei, H.; Okada, O.; Takigawa, T.; Ohmura, N.; Matsumiya, N.; Matsuyama, H. Selective Separation of CO_2 by Using Novel Facilitated Transport Membrane at Elevated Temperatures and Pressures. *J. Membr. Sci.* **2007**, *291*, 157−164.

(17) Arslan, O.; Dogan, S. Inhibition of Polyphenol Oxidase Obtained From Various Sources by 2, 3−Diaminopropionic Acid. *J. Sci. Food Agric.* **2005**, *85*, 1499−1504.

(18) Koh, H.; Lau, A.; Chan, E. C. Hydrophilic Interaction Liquid Chromatography with Tandem Mass Spectrometry for the Determination of Underivatized Dencichine (β−N−Oxalyl−L−α,β−Diaminopropionic Acid) in Panax Medicinal Plant Species. *Rapid Commun. Mass Spectrom.* **2005**, *19*, 1237−1244.

(19) Wang, X.; Gan, H.; Zhang, M.; Sun, T. Modulating Cell Behaviours on Chiral Polymer Brush Films with Different Hydrophobic Side Groups. *Langmuir* **2012**, *28*, 2791−2798.

(20) Wang, X.; Gan, H.; Sun, T. Chiral Design for Polymeric Biointerface: The Influence of Surface Chirality on Protein Adsorption. *Adv. Funct. Mater.* **2011**, *21*, 3276−3281.

(21) El-Gindi, J.; Benson, K.; De Cola, L.; Galla, H. J.; Kehr, N. S. Cell Adhesion Behavior on Enantiomerically Functionalized Zeolite L Monolayers. *Angew. Chem., Int. Ed.* **2012**, *51*, 3716−3720.

(22) Liu, G.; Zhang, D.; Feng, C. Control of Three-Dimensional Cell Adhesion by the Chirality of Nanofibers in Hydrogels. *Angew. Chem., Int. Ed.* **2014**, *53*, 7789−7793.

(23) Hummers, W. S., Jr; Offeman, R. E. Preparation of Graphitic Oxide. *J. Am. Chem. Soc.* **1958**, *80*, 1339−1339.

(24) Hu, H.; Zhao, Z.; Wan, W.; Gogotsi, Y.; Qiu, J. Ultralight and Highly Compressible Graphene Aerogels. *Adv. Mater.* **2013**, *25*, 2219−2223.

(25) Chen, J.; Sheng, K.; Luo, P.; Li, C.; Shi, G. Graphene Hydrogels Deposited in Nickel Foams for High-Rate Electrochemical Capacitors. *Adv. Mater.* **2012**, *24*, 4569−4573.

(26) McAllister, M. J.; Li, J.; Adamson, D. H.; Schniepp, H. C.; Abdala, A. A.; Liu, J.; Herrera-Alonso, M.; Milius, D. L.; Car, R.; Prud'homme, R. K.; Aksay, I. A. Single Sheet Functionalized Graphene by Oxidation and Thermal Expansion of Graphite. *Chem. Mater.* **2007**, *19*, 4396−4404.

(27) Jhong, J.; Venault, A.; Hou, C.; Chen, S.; Wei, T.; Zheng, J.; Huang, J.; Chang, Y. Surface Zwitterionization of Expanded Poly-(tetrafluoroethylene) Membranes via Atmospheric Plasma-Induced Polymerization for Enhanced Skin Wound Healing. *ACS Appl. Mater. Interfaces* **2013**, *5*, 6732−6742.

(28) Shih, M. F.; Shau, M. D.; Chang, M. Y.; Chiou, S. K.; Chang, J. K.; Cherng, J. Y. Platelet Adsorption and Hemolytic Properties of Liquid Crystal/Composite Polymers. *Int. J. Pharm.* **2006**, *327*, 117−125.

(29) Ong, S. Y.; Wu, J.; Moochhala, S. M.; Tan, M. H.; Lu, J. Development of a Chitosan-Based Wound Dressing with Improved Hemostatic and Antimicrobial Properties. *Biomaterials* **2008**, *29*, 4323−4332.

(30) Sudheesh Kumar, P. T.; Lakshmanan, V. K.; Anilkumar, T. V.; Ramya, C.; Reshmi, P.; Unnikrishnan, A. G.; Nair, S. V.; Jayakumar, R. Flexible and Microporous Chitosan Hydrogel/Nano ZnO Composite Bandages for Wound Dressing: in Vitro and in Vivo Evaluation. *ACS Appl. Mater. Interfaces* **2012**, *4*, 2618−2629.

(31) Behrens, A. M.; Sikorski, M. J.; Li, T.; Wu, Z. J.; Griffith, B. P.; Kofinas, P. Blood-aggregating Hydrogel Particles for Use as a Hemostatic Agent. *Acta Biomater.* **2014**, *10*, 701−708.

(32) Luo, L.; Li, G.; Luan, D.; Yuan, Q.; Wei, Y.; Wang, X. Antibacterial Adhesion of Borneol-Based Polymer via Surface Chiral Stereochemistry. *ACS Appl. Mater. Interfaces* **2014**, *6*, 19371−19377.

(33) Lv, R.; Gai, S.; Dai, Y.; Niu, N.; He, F.; Yang, P. Highly Uniform Hollow GdF_3 Spheres: Controllable Synthesis, Tuned Luminescence, and Drug-Release Properties. *ACS Appl. Mater. Interfaces* **2013**, *5*, 10806−10818.

(34) Shi, Z.; Zhang, W.; Zhang, F.; Liu, X.; Wang, D.; Jin, J.; Jiang, L. Ultrafast Separation of Emulsified Oil/Water Mixtures by Ultrathin Free-Standing Single-Walled Carbon Nanotube Network Films. *Adv. Mater.* **2013**, *25*, 2422−2427.

(35) Bi, H.; Xie, X.; Yin, K.; Zhou, Y.; Wan, S.; He, L.; Xu, F.; Banhart, F.; Sun, L.; Ruoff, R. S. Spongy Graphene as a Highly Efficient and Recyclable Sorbent for Oils and Organic Solvents. *Adv. Funct. Mater.* **2012**, *22*, 4421−4425.

(36) Gegel, B. T.; Burgert, J. M.; Lockhart, C.; Austin, R.; Davila, A.; Deeds, J.; Hodges, L.; Hover, A.; Roy, J.; Simpson, G.; Weaver, S.; Wolfe, W.; Johnson, D. Effects of Celox and TraumaDEX on Hemorrhage Control in a Porcine Model. *AANA J.* **2010**, *78*, 115−120.

(37) Park, Y. I.; Kim, H. M.; Kim, J. H.; Moon, K. C.; Yoo, B.; Lee, K. T.; Lee, N.; Choi, Y.; Park, W.; Ling, D.; Na, K.; Moon, W. K.; Choi, S. H.; Park, H. S.; Yoon, S.-Y.; Suh, Y. D.; Lee, S. H.; Hyeon, T. Theranostic Probe Based on Lanthanide-Doped Nanoparticles for Simultaneous In Vivo Dual-Modal Imaging and Photodynamic Therapy. *Adv. Mater.* **2012**, *24*, 5755−5761.

(38) Wang, L.; Xing, H.; Zhang, S.; Ren, Q.; Pan, L.; Zhang, K.; Bu, W.; Zheng, X.; Zhou, L.; Peng, W.; Hua, Y.; Shi, J. A Gd-doped Mg-Al-LDH/Au Nanocomposite for CT/MR Bimodal Imagings and Simultaneous Drug Delivery. *Biomaterials* **2013**, *34*, 3390−3401.